


Cite this: *RSC Adv.*, 2019, 9, 13112

Immobilized antimony species on magnetite: a novel and highly efficient magnetically reusable nanocatalyst for direct and gram-scale reductive-coupling of nitroarenes to azoarenes†

Behzad Zeynizadeh * and Fariba Faraji

In this study, magnetic nanoparticles of $\text{Fe}_3\text{O}_4@\text{SbF}_x$ from the immobilization of SbF_3 on magnetite were synthesized. The prepared nanocomposite system was then characterized using scanning electron microscopy, Fourier transform infrared spectroscopy, X-ray diffraction, energy-dispersive X-ray spectroscopy, vibrating sample magnetometry and inductively coupled plasma optical emission spectroscopy. Next, the catalytic activity of $\text{Fe}_3\text{O}_4@\text{SbF}_x$ MNPs was highlighted by one-pot reductive-coupling of aromatic nitro compounds to the corresponding azoarene materials with NaBH_4 . The reactions were carried out in refluxing EtOH within 6–25 min to afford the products in high yields. The reusability of the Sb-magnetite system was also studied for 6 consecutive cycles without significant loss of catalytic activity. This synthetic protocol provided several advantages in terms of introducing a novel catalytic system based on antimony species for direct and gram-scale preparation of azoarenes from nitroarenes, low loading of the nanocatalyst, mild reaction conditions, using ethanol as a green and economic solvent and high yield of the products.

Received 18th February 2019
Accepted 23rd April 2019

DOI: 10.1039/c9ra01249d

rsc.li/rsc-advances

Introduction

Synthesis of azoarenes is one of the valuable topics in organic synthesis. These materials have widespread capabilities and are utilized in numerous fields of modern technologies such as synthesis of organic dyes and pigments,^{1–3} and as initiators of radical reactions,⁴ food additives, indicators⁵ and drug delivery systems.⁶ They possess excellent photoelectric and optic-memory properties.⁷ The recent studies also show that azobenzenes were successfully used in image storage and optical switches,⁸ molecular shuttles based on a rotaxane,⁹ nanotubes,¹⁰ electronic devices¹¹ and production of filters as well as protection of eye glasses.¹² Due to the *cis-trans* isomerization of the azo functionality by adequate radiation, azobenzenes were also used in photochemical molecular switches¹³ and photoregulation of DNA triplex formation.¹⁴ It was also reported that azoarenes can play a crucial role in the development of synthetic¹⁵ and mechanistic organic chemistry.¹⁶ Based on these great capabilities, much attention has been devoted to the synthesis of azobenzenes by various methods.

The literature review shows that the multistep synthesis of azoarene materials was primarily carried out through the coupling of diazonium ions¹⁷ and Anson reaction.¹⁸ In due

course, the multistep preparation of azoarenes has been extensively reviewed by Merino.¹⁹ Although most of the reported protocols provided the useful synthetic capabilities, however, they generally suffer from low to moderate yield of the products, the prolonged reaction times, cyclization, isomerization and rearrangement reactions.^{20,21} To overcome the mentioned shortcomings, several synthetic methods through the improvement of the catalyst activity have been reported.^{22,23} In contrast to the multistep strategy, the straightforward oxidative-coupling of aromatic amines to azoarenes^{24–26} and reductive-coupling of nitroarenes to azoxyarenes^{27–33} was also a subject of more interest. In this context, the application of $\text{HCOONH}_4/\text{Pb}$,³⁴ $\text{CH}_3\text{COONH}_4/\text{Pb}$,³⁵ $\text{HCOONH}_4/\text{Pb}$,³⁶ $\text{HCOONH}_4/\text{Mg}$,³⁷ LiAlH_4 ,³⁸ $\text{NaH}_2\text{Al}(\text{OCH}_2\text{CH}_2\text{OMe})_2$,³⁹ $\text{NaBH}_4/\text{DMSO}$,⁴⁰ $(\text{MeCN})_3\text{-Cr}(\text{CO})_3$,⁴¹ $\text{Co}_2(\text{CO})_8$,⁴² $\text{HOCH}_2\text{CH}_2\text{ONa}$,⁴³ Zn/NaOH ,⁴⁴ Bi/KOH ,⁴⁵ $\text{Mg}/\text{NH}_4\text{Br}$,⁴⁶ Mg/MeOH ,⁴⁷ Mg/MCl_n (MCl_n : TiCl_4 , VCl_3 , CrCl_3 , MoOCl_3 , WCl_6 and FeCl_3),⁴⁸ $\text{Pd}(\text{acac})_2/\text{H}_2$,⁴⁹ $\text{InBr}_3/\text{Et}_3\text{SiH}$,⁵⁰ $\text{In}(\text{OTf})_3/\text{Et}_3\text{SiH}/\text{O}_2$,⁵¹ $\text{FeCl}_2 \cdot 4\text{H}_2\text{O}/\text{Li}/\text{DTBB}$,⁵² electro-reduction,⁵³ $\text{Au}/\text{meso CeO}_2/\text{CO}$,⁵⁴ Li/THF ,⁵⁵ $\text{Bi}/\text{ball mill}$ ⁵⁶ and Cr ⁵⁷ has also been documented for direct conversion of nitroarenes to azoarene materials.

It is also known that in the promoted reactions by metal nanoparticles, the electronic influence of metal species, nano-size dimension of particles and porosity of the surface play the synergic roles to improve the rate of examined reactions. However, metal nanoparticles generally due van der Waals, electrostatic or magnetic forces represent a strong tendency for agglomeration

Faculty of Chemistry, Urmia University, Urmia 5756151818, Iran. E-mail: bzeynizadeh@gmail.com; Fax: +98-44-32755294; Tel: +98-44-32755294

† Electronic supplementary information (ESI) available. See DOI: 10.1039/c9ra01249d



while it decreases the active surface area and catalytic activity of the applied catalyst system. In order to overcome this shortcoming and preserve the original characteristics of nanoparticles, the immobilization of metal nanoparticles on organic and inorganic stabilizers/supports has been frequently documented. Organic ligand,⁵⁸ polymer,⁵⁹ zeolites,^{60,61} reduced graphene oxide,^{62–65} CuO,⁶⁶ gums⁶⁷ and magnetic materials⁶⁸ are the stabilizers which have been successfully served for the immobilization of metal nanoparticles. Among these, the magnetic nanoparticles (MNPs) of Fe₃O₄ due extreme specific surface area, high magnetic property, chemical solidity and ease of preparation and separation are more appropriate for anchoring the metal species.⁶⁹

In line with the outlined strategies and continuation of our research program directed to synthetic usefulness of magnetic nanocatalysts,^{70–76} herein, we wish to report synthesis of the immobilized antimony species on magnetite, Fe₃O₄@SbF_x, as novel, highly efficient and reusable magnetic nanocatalyst for straightforward reductive-coupling of nitroarenes to symmetrically substituted azoarene materials in refluxing EtOH (Scheme 1).

Results and discussion

Preparation and characterization of Fe₃O₄@SbF_x MNPs

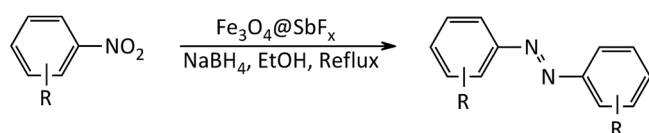
The study was started by preliminary preparation of magnetically nanoparticles of Fe₃O₄@SbF_x with 15% Sb species *via* a two-step procedure: (i) preparation of Fe₃O₄ MNPs by chemical co-precipitation of FeCl₃·6H₂O and FeCl₂·4H₂O in aqueous ammonia and (ii) the immobilization of SbF_x on magnetite by simply mixing of an aqueous solution of SbF₃ with Fe₃O₄ MNPs under reflux conditions (Scheme 2).

Characterization of Fe₃O₄@SbF_x MNPs

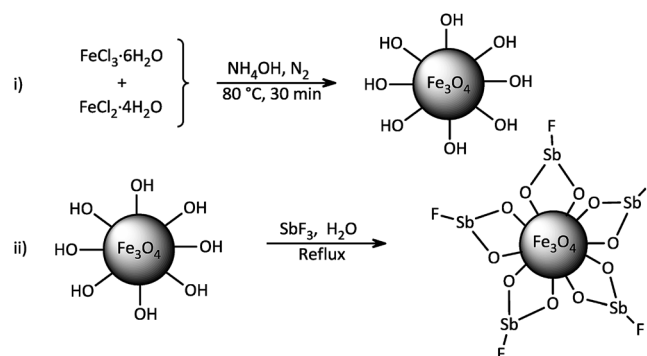
After the successful synthesis of Fe₃O₄@SbF_x MNPs, the nanocatalyst was then characterized using Fourier transform infrared spectroscopy (FT-IR), scanning electron microscopy (SEM), energy-dispersive X-ray spectroscopy (EDX), X-ray diffraction (XRD), vibrating sample magnetometer (VSM), N₂ adsorption-desorption analysis and inductively coupled plasma-optical emission spectroscopy (ICP-OES).

FT-IR analysis

Fourier transform infrared spectroscopy as a primarily tool was used for structural elucidation of Fe₃O₄ and Fe₃O₄@SbF_x MNPs. In this context, FT-IR spectrum of Fe₃O₄ (Fig. 1a) shows a strong absorption band at 575 cm⁻¹ showing the stretching vibration of Fe–O bond. The absorption peaks at 1625 and 3400 cm⁻¹ are also attributed to O–H deforming and stretching vibrations of adsorbed water, respectively. FT-IR spectrum of Fe₃O₄@SbF_x MNPs (Fig. 1b) also



Scheme 1 Synthesis of azoarenes catalyzed by NaBH₄/Fe₃O₄@SbF_x MNPs system.



Scheme 2 Synthesis of magnetically nanoparticles of Fe₃O₄@SbF_x.

shows the absorption peaks at 3421 and 1631 cm⁻¹ related to the stretching and bending vibrations of OH groups on the surface of nanoparticles. The peaks around 1021 and 566 cm⁻¹ are respectively attributed to stretching vibrations of Sb–O and Sb–F bonds. Therefore, the later absorption bands successfully verify the immobilization of SbF_x species on the surface of magnetite.

SEM analysis

Morphology of the surface and size distribution of nanoparticles in Fe₃O₄ and Fe₃O₄@SbF_x MNPs were also investigated using scanning electron microscopy technique (Fig. 2). The surface-microscopy image of Fe₃O₄ MNPs (Fig. 2a) represents that the magnetite was constituted from uniform and ultrafine granular particles distributed in the range of 10–21 nm. As well, SEM image of Fe₃O₄@SbF_x MNPs (Fig. 2b) shows that through the reaction of magnetite with SbF₃, the surface of Sb-magnetite was thoroughly modified and constituted from porous and uniform granular nanoparticles distributed in the range of 45–68 nm.

EDX analysis

Energy-dispersive X-ray (EDX) spectroscopy as an effective technique was used to determine the presence of elements in a material. According to the depicted graphs for EDX analysis of Fe₃O₄ and Fe₃O₄@SbF_x MNPs (Fig. 3), the presence of Fe and O in Fe₃O₄ as well Fe, O, Sb and F elements in Fe₃O₄@SbF_x MNPs

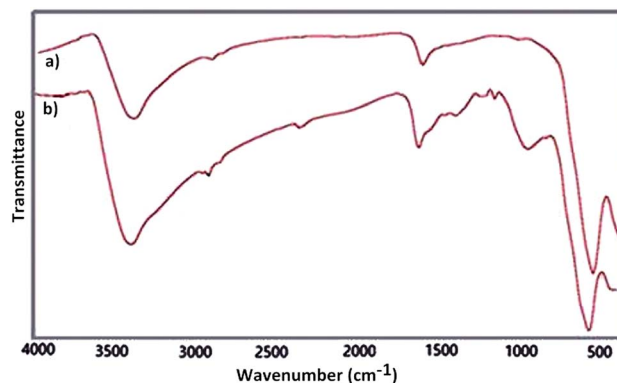


Fig. 1 FT-IR spectra of (a) Fe₃O₄ and (b) Fe₃O₄@SbF_x MNPs.



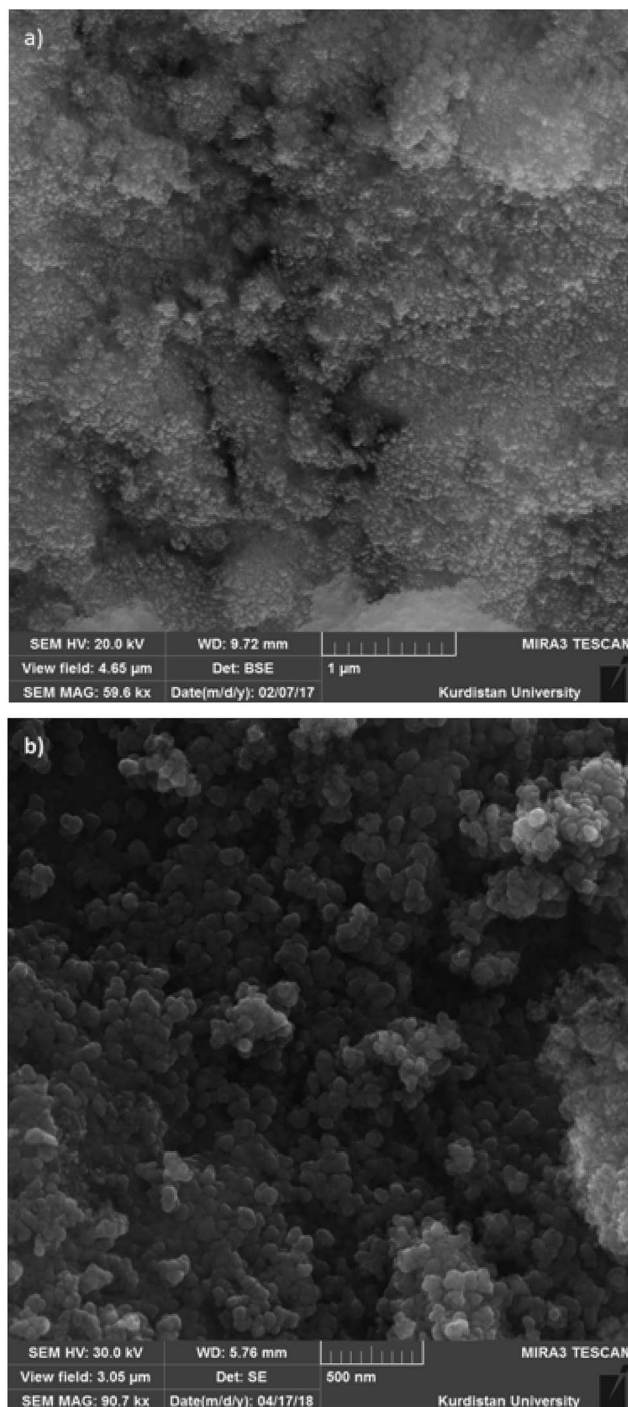


Fig. 2 SEM images of (a) Fe_3O_4 and (b) $\text{Fe}_3\text{O}_4@\text{SbF}_x$ MNPs.

is proved. This analysis clearly shows the successful immobilization of SbF_x species on the surface of Fe_3O_4 .

ICP-OES analysis

In continuation to EDX analysis, the exact amounts of Fe and Sb in $\text{Fe}_3\text{O}_4@\text{SbF}_x$ MNPs were determined by inductively coupled plasma optical emission spectroscopy (ICP-OES). Based on this analysis, the amounts of Sb and Fe in $\text{Fe}_3\text{O}_4@\text{SbF}_x$ MNPs were found to be 15.06% and 54.1%, respectively.

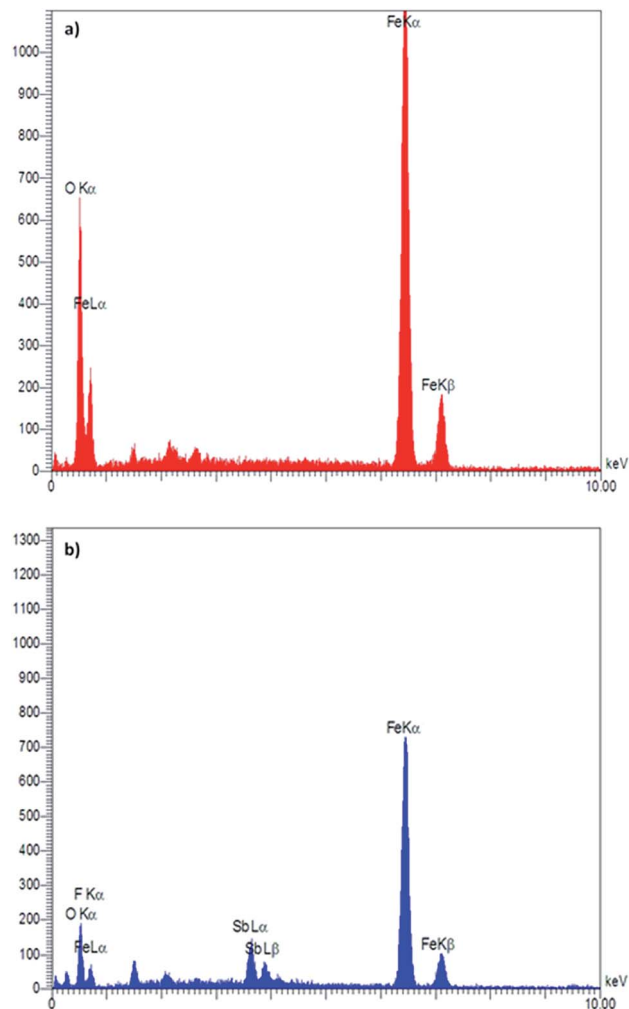


Fig. 3 EDX spectra of (a) Fe_3O_4 and (b) $\text{Fe}_3\text{O}_4@\text{SbF}_x$ MNPs.

XRD analysis

At the next, the phase purity and crystallinity structure of the prepared nanocatalysts was determined using X-ray diffraction (XRD) analysis. Fig. 4 represents XRD diffractograms of Fe_3O_4 and $\text{Fe}_3\text{O}_4@\text{SbF}_x$ MNPs. In XRD pattern of Fe_3O_4 , the peaks at $2\theta = 30.2^\circ$, 35.5° , 43.3° , 53.7° , 57.2° and 62.9° are attributed to (220), (311), (400), (422), (511) and (440) reflection planes of cubic spinel Fe_3O_4 (JCPDS 65-3107).^{77,78} In XRD pattern of $\text{Fe}_3\text{O}_4@\text{SbF}_x$ MNPs (Fig. 4b), the presence of characteristic peaks related to Fe_3O_4 is verifying that during the immobilization of Sb species, no structural change has been taken place in the spinel structure of magnetite. Moreover, the absorption peak at $2\theta = 26^\circ$ is exactly attributed to the bond of Sb–F showing the immobilization of Sb species on the surface of Fe_3O_4 MNPs.⁷⁹

BET analysis

The porosity and surface characteristics of $\text{Fe}_3\text{O}_4@\text{SbF}_x$ MNPs was studied through the N_2 adsorption–desorption analysis. The results of this investigation are illustrated in Fig. 5. According to categories of adsorption isotherms (BDDT), the shape of isotherm for $\text{Fe}_3\text{O}_4@\text{SbF}_x$ MNPs is belonged to type of



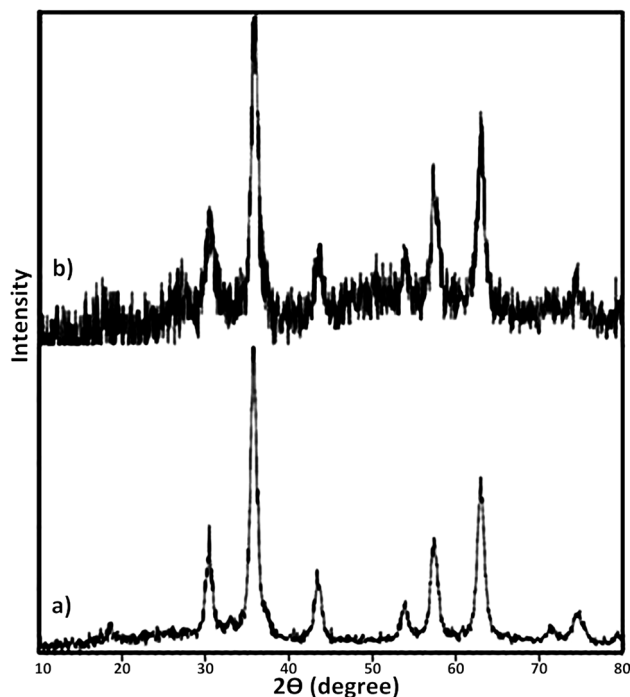


Fig. 4 XRD diffractograms of (a) Fe_3O_4 and (b) $\text{Fe}_3\text{O}_4@\text{SbF}_x$ MNPs.

IV with H3 hysteresis loop of desorption pathway. This type of isotherm is a characteristic of mesoporous materials. Table 1 represents total pore volume (V_{total}), pore diameter (D_{BJH}) and BET surface area (S_{BET}) of $\text{Fe}_3\text{O}_4@\text{SbF}_x$ MNPs. Investigation of the results shows that through modifying of the magnetite with SbF_x species, porosity of the surface was increased. Subsequently, the specific surface area was raised to $75.7 \text{ m}^2 \text{ g}^{-1}$ followed by decreasing the pores diameter to 5.74 nm.

VSM analysis

Magnetic property of Fe_3O_4 and $\text{Fe}_3\text{O}_4@\text{SbF}_x$ MNPs were also studied by vibrating sample magnetometer (VSM) analysis in the applied magnetic field up to 20 kOe (Fig. 6). The saturation magnetization (M_s) value of Fe_3O_4 (Fig. 6a) and $\text{Fe}_3\text{O}_4@\text{SbF}_x$ (Fig. 6b) were found to be 66.976 and $23.229 \text{ emu g}^{-1}$, respectively. The graphs are clearly showing that through the immobilization of SbF_x species on the surface of magnetite, M_s value of $\text{Fe}_3\text{O}_4@\text{SbF}_x$ was notably decreased. However, the magnetization value was still large enough for any magnetic separation.

One-pot reductive-coupling of nitroarenes to azoarenes with NaBH_4 catalyzed by $\text{Fe}_3\text{O}_4@\text{SbF}_x$ MNPs

After the successful synthesis and characterization of the antimony-coated magnetite, catalytic activity of the prepared nanocatalyst was further investigated towards one-pot reductive-coupling of aromatic nitro compounds to the corresponding azoarenes.

The study was started with the preliminary aim of using antimony-coated magnetite as a catalyst towards reduction of nitroarenes to the corresponding anilines with NaBH_4 . Therefore, reduction of nitrobenzene with NaBH_4 (as a model

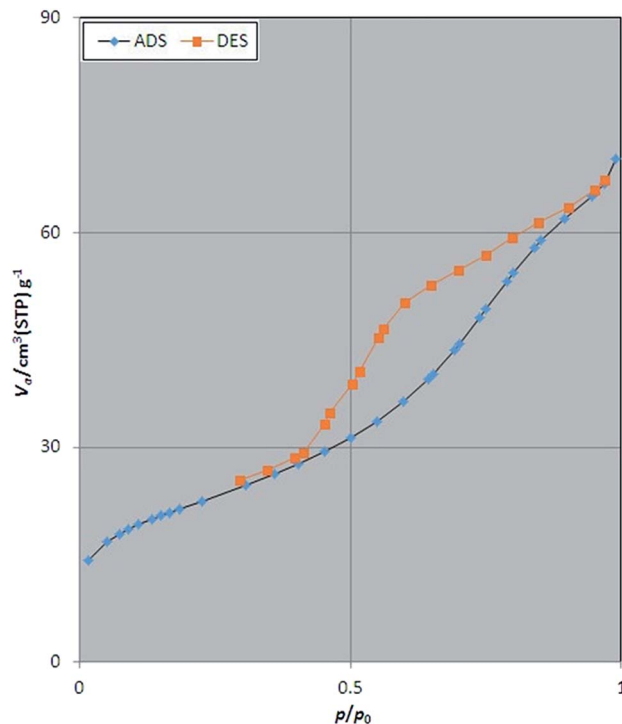


Fig. 5 N_2 adsorption-desorption isotherm of $\text{Fe}_3\text{O}_4@\text{SbF}_x$ MNPs.

reaction) in the presence and absence of antimony-coated magnetite was investigated with the change of reaction-solvent and amounts of nanocatalyst as well as verifying the influence of temperature (Table 2). The results of this study exhibited that progress of the reaction in the absence of Sb-nanocatalyst led to unsatisfactory yield of the product. However, the influence of small amounts of nanocatalyst on the

Table 1 The surface analysis of $\text{Fe}_3\text{O}_4@\text{SbF}_x$ MNPs

Sample	S_{BET} ($\text{m}^2 \text{ g}^{-1}$)	Pore diameter (nm)	Total pore volume ($\text{cm}^3 \text{ g}^{-1}$)
$\text{Fe}_3\text{O}_4@\text{SbF}_x$ MNPs	75.739	5.738	0.1086

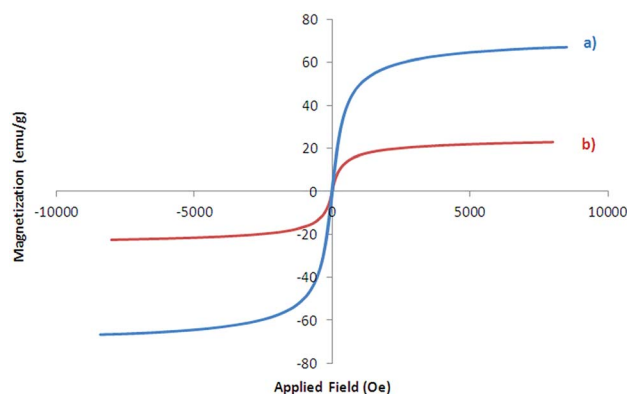


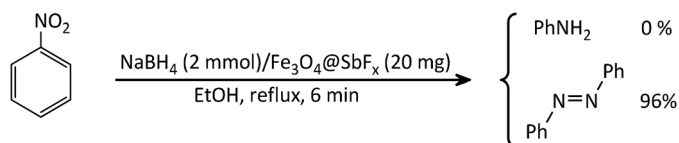
Fig. 6 Magnetization curves of (a) Fe_3O_4 and (b) $\text{Fe}_3\text{O}_4@\text{SbF}_x$ MNPs.



Table 2 Optimization experiments for reductive-coupling of nitrobenzene to azobenzene with NaBH₄/Fe₃O₄@SbF_x MNPs system^a

Entry	NaBH ₄ (mmol)	Fe ₃ O ₄ @SbF _x (mg)	Solvent (2 mL)	Condition	Time (min)	Conversion (%)
1	2	—	H ₂ O	Reflux	240	—
2	1	10	H ₂ O	Reflux	120	40
3	2	10	H ₂ O	Reflux	120	60
4	2	20	H ₂ O	Reflux	45	100
5	2	20	H ₂ O–EtOH (1 : 1)	Reflux	300	100
6	2	20	EtOH	Reflux	6	100
7	2	20	CH ₃ CN	Reflux	120	30

^a All reactions were carried out with 1 mmol of nitrobenzene.

Scheme 3 Reductive-coupling of nitrobenzene to azobenzene with NaBH₄/Fe₃O₄@SbF_x MNPs.

rate of reaction was noteworthy. In addition, it was very amazing that the product of reaction was azobenzene while it was expected to obtain aniline as a product. This transformation was clearly identifiable through the color change of the reaction to

orange-red solution. As well, instrumental analysis also verified the formation of azobenzene as a sole product. The examinations represented that using NaBH₄ (2 mmol) and Fe₃O₄@SbF_x MNPs (20 mg) in refluxing EtOH as a green and economic solvent was sufficient to perform one-pot reductive-coupling of nitrobenzene (1 mmol) to azobenzene within 6 min and 96% isolated yield (Scheme 3) (Table 2, entry 6).

At the next, the generality and usefulness of this synthetic protocol was further studied using structurally diverse aromatic nitro compounds at the optimized reaction conditions (Table 2, entry 6). The results of this investigation are summarized in Table 3. The table shows that all reductive-coupling of nitroarenes containing electron-withdrawing and releasing

Table 3 Reductive-coupling of nitroarenes with NaBH₄/Fe₃O₄@SbF_x system^a

Entry	Product	Time (min)	Yield ^b (%)	Mp ³⁴ (°C)
1		6	95	67–68
2		10	92	54–56
3		12	93	55–56
4		14	94	144–145

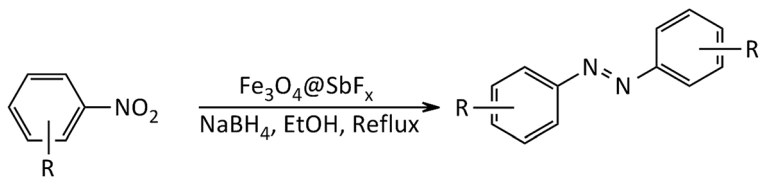
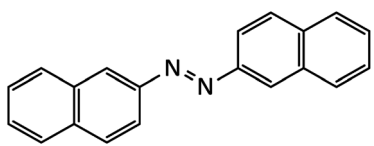


Table 3 (Contd.)

Entry	Product	Time (min)	Yield ^b (%)	Mp ³⁴ (°C)
5		40	91	214–215
6		16	94	136–138
7		18	96	101–102
8		20	95	187–188
9		8	92	130–132
10		10	89	90–92
11		8	94	160–162
12		25	93	190–191



Table 3 (Contd.)

				
Entry	Product	Time (min)	Yield ^b (%)	Mp ³⁴ (°C)
13		15	94	207–209

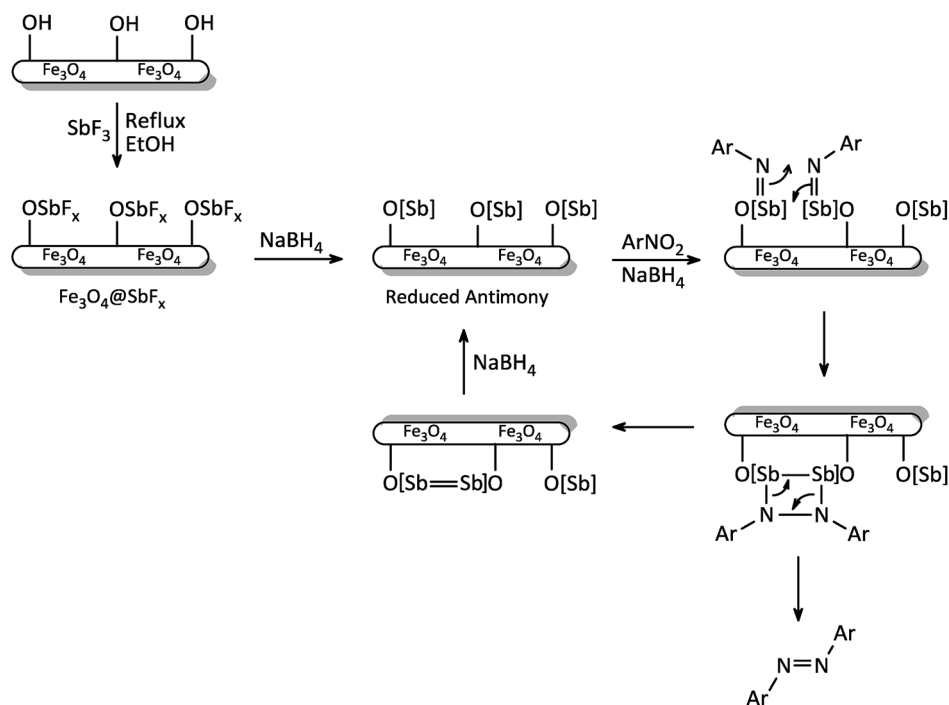
^a All reactions were carried out with the molar ratio of subs./NaBH₄ (1 : 2) in the presence of Fe₃O₄@SbF_x (20 mg) in refluxing EtOH (2 mL). ^b Yields refer to isolated pure products.

functionalities were carried out successfully using NaBH₄ (2 mmol)/Fe₃O₄@SbF_x (0.02 g) in refluxing ethanol within 6–25 min giving the corresponding azoarene materials in high yields. In addition, the capability of this protocol for gram scale synthesis of azoarene materials was also investigated by one-pot reductive-coupling of nitrobenzene (1.0 g, 8.1 mmol) with NaBH₄ (0.61 g, 16 mmol)/Fe₃O₄@SbF_x (160 mg) in refluxing EtOH (5 mL). The obtained result exhibited that the reaction was taken place successfully within 10 min to afford azobenzene in 94% yield (0.7 g).

The exact mechanism of this synthetic protocol is not clear; however, a depicted mechanism (Scheme 4) shows a pathway for the influence of NaBH₄/Fe₃O₄@SbF_x system on one-pot reductive-

coupling of nitroarenes to azoarene materials. The scheme shows that the Sb-magnetite nanocatalyst in the presence of NaBH₄ was converted to the reduced-antimony species. Through the reaction of this activated nanocatalyst with nitroarene, the formation of imino-antimony intermediate was carried out. At the next, through the [2 + 2] cycloaddition reaction of two imino-antimony species followed by skeletal rearrangement, the formation of azoarenes product was taken place.

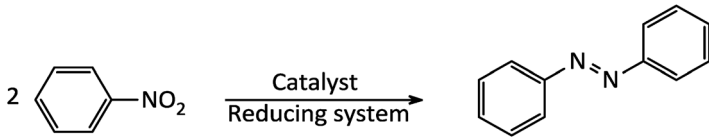
In order to show the suitability and usefulness of NaBH₄/Fe₃O₄@SbF_x system towards one-pot synthesis of azoarene materials, the result of reductive-coupling of nitrobenzene to azobenzene was compared with the previously reported procedures (Table 4). An



Scheme 4 The proposed mechanism for reductive-coupling of nitroarenes to azoarenes with NaBH₄/Fe₃O₄@SbF_x system.



Table 4 Reductive-coupling of nitrobenzene to azobenzene with $\text{NaBH}_4/\text{Fe}_3\text{O}_4@\text{SbF}_x$ and other reported systems

						
Entry	Catalyst system	Condition	Time (min)	Yield (%)	Reusability	Ref.
1	$\text{NaBH}_4/\text{Fe}_3\text{O}_4@\text{SbF}_x$	EtOH/reflux	6	95	6	^a
2	$\text{HCO}_2\text{NH}_4/\text{Pb}$	MeOH/reflux	60	92	—	34
3	$\text{HCO}_2\text{HNEt}_3/\text{Pb}$	MeOH/r.t.	120	92	—	36
4	LiAlH_4	$\text{Et}_2\text{O}/-80^\circ\text{C}$	—	84	—	38
5	NaBH_4	DMSO/ 85°C	90	75	—	40
6	$\text{HOCH}_2\text{CH}_2\text{ONa}$	Ethylene glycol	3	88	—	43
7	Bi/KOH	MeOH/microwave	8	85	—	45
8	$\text{Mg}/\text{NH}_4\text{Br}$	MeOH/r.t.	90	90	—	46
9	$\text{Pd}(\text{acac})_2/\text{H}_2$ (1 atm)	$\text{KOH}/70^\circ\text{C}/\text{EtOH}$	360	90	—	49
10	$\text{In}(\text{OTf})_3\text{-Et}_3\text{SiH}$	$\text{O}_2/\text{DMF}/60^\circ\text{C}$	720	84	—	51
11	$\text{FeCl}_2\cdot 4\text{H}_2\text{O}/\text{Li}/\text{DTBB}$	THF/reflux	150	97	—	52
12	$\text{Au}/\text{meso-CeO}_2/\text{CO}$ (5 atm)	Toluene/ 150°C	300	99	—	54

^a Present work.

investigation shows that in terms of the amount of nanocatalyst, mild reaction conditions, selective formation of azobenzene, short reaction time, high yield of the product and great reusability of the Sb-nanocatalyst, the current system represents the outstanding advantages.

Recyclability of $\text{Fe}_3\text{O}_4@\text{SbF}_x$ MNPs

Nowadays, the recovery and reusability of the applied catalyst system has become a crucial subject in academic and industrial points of view. The green and economic aspect of this synthetic method was also studied by investigation of the reusability of $\text{Fe}_3\text{O}_4@\text{SbF}_x$ MNPs in reductive-coupling of nitrobenzene to azobenzene with NaBH_4 at the optimized reaction conditions (Table 2, entry 6). After completion of the reaction, the Sb-magnetite nanocatalyst was magnetically recovered from the reaction mixture, washed with EtOAc and then dried for reusing

at the next runs. The model reaction was again charged with the fresh NaBH_4 , nitrobenzene, ethanol and the recovered Sb-nanocatalyst. Fig. 7 shows that the nanocatalyst can be reused for six consecutive cycles without the significant loss of catalytic activity. It is also notable that due small decreasing in the activity of nanocatalyst and therefore remaining of the starting material for 1–5% over the six recycling of the nanocatalyst, isolated yield of the product was reduced for 1–5% in respect to the first run of model reaction (96%).

Conclusions

In this study, magnetically nanoparticles of the novel antimony-coated magnetite, $\text{Fe}_3\text{O}_4@\text{SbF}_x$, were prepared. The prepared nanocomposite was then characterized using FT-IR, SEM, EDX, XRD, BET, VSM and ICP analyses. The heterogeneous Sb-nanocatalyst showed an extraordinary catalytic activity toward rapid and efficient reductive-coupling of nitroarenes to azoarene materials with NaBH_4 in refluxing ethanol as a green solvent. All reactions were carried out using NaBH_4 (2 mmol)/ $\text{Fe}_3\text{O}_4@\text{SbF}_x$ (20 mg) within 6–25 min to give the products in high yields. This synthetic protocol offers numerous advantages in terms of the novel and easy synthesis of Sb-magnetite nanocatalyst, mild reaction conditions in comparison to the previously reported methods, using EtOH as green solvent, short reaction times, high yield of the products, simple work-up procedure and the great reusability of the nanocatalyst.

Experimental

Chemicals and apparatus

All chemicals in analytical grade were purchased from chemical companies and were used without further purification. FT-IR and ^1H , ^{13}C NMR spectra were recorded on Thermo Nicolet

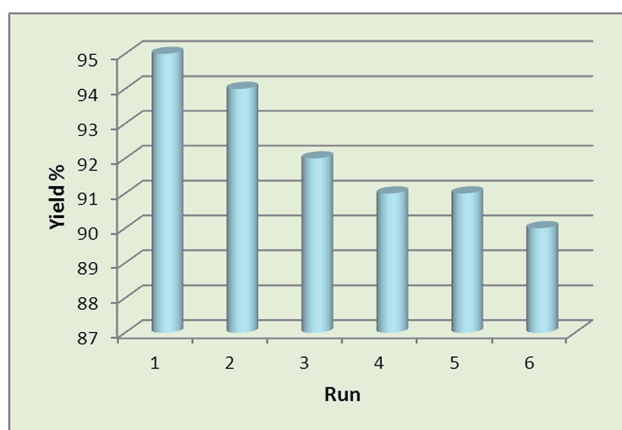


Fig. 7 Reusability of $\text{Fe}_3\text{O}_4@\text{SbF}_x$ MNPs in reductive-coupling of PhNO_2 with NaBH_4 .



Nexus 670 and Bruker Avance 300 MHz spectrometers, respectively. Melting points were measured on Electrothermal 9100 apparatus and were uncorrected. Mass spectra of the samples were obtained from Mass spectrometer (Agilent, 5975C, 20–70 eV). Morphology and size distribution of nanoparticles were determined by scanning electron microscopy (SEM) using FESEM-TESCAN followed by energy-dispersive X-ray analysis (EDX). Magnetic property of materials were measured by vibrating sample magnetometer (VSM, model MDKFT) under magnetic fields up to 20 kOe. Elemental composition of the samples was determined using inductively coupled plasma-optical emission spectrometer (ICP-OES). Specific surface area and pore size distribution of nanoparticles were determined on Belsorp-Max (Japan) instrument using N₂ adsorption-desorption isotherm. X-ray diffraction (XRD) analysis was carried out by X'PertPro diffractometer. TLC was applied for monitoring of the reactions over silica gel 60 F254 aluminum sheet. All products were identified by physical and spectral data followed by comparison with authentic data.

Preparation of Fe₃O₄ MNPs

Magnetically nanoparticles of Fe₃O₄ were prepared *via* a chemical co-precipitation protocol.⁷⁰ Due course, a solution of FeCl₃·6H₂O (0.0216 mol, 5.838 g) and FeCl₂·4H₂O (0.0108 mol, 2.147 g) in deionized water (100 mL) was prepared. The solution was stirred for 10 min at 85 °C under N₂ atmosphere. Next, aqueous ammonia (25%, 10 mL) was quickly added and the black nanoparticles of Fe₃O₄ were instantly precipitated. The resulting mixture was again stirred for 30 min at 85 °C under N₂ atmosphere. The mixture was cooled to the room temperature and Fe₃O₄ MNPs were magnetically separated from the reaction mixture. The nanoparticles were washed with distilled water, a solution of NaCl (0.02 M) and again with distilled water. Drying under air atmosphere afforded the nanoparticles of Fe₃O₄.

Synthesis of Fe₃O₄@SbF_x MNPs

To a solution of SbF₃ (0.15 g, 0.84 mmol) in deionized water (20 mL), magnetically nanoparticles of Fe₃O₄ (0.5 g, 2.15 mmol) was added. The resulting suspension was stirred for 20 h at 80 °C. After that, magnetically nanoparticles of Fe₃O₄@SbF_x were separated by an external magnetic field, washed with deionized water and then dried at 60 °C.

A typical procedure for reductive-coupling of nitrobenzene to azobenzene with NaBH₄/Fe₃O₄@SbF_x MNPs

A mixture of nitrobenzene (0.123 g, 1 mmol) and Fe₃O₄@SbF_x (0.02 g) in EtOH (3 mL) was well stirred for 2 min. NaBH₄ (0.076 g, 2 mmol) was then added and the resulting mixture was stirred under reflux conditions for 6 min. During the progress of the reaction, the color of mixture was changed to orange-red showing the formation of azobenzene product. After completion of the reaction (monitored by TLC, *n*-hexane/EtOAc: 10/2), the mixture was cooled to the room temperature. The nanocatalyst was magnetically separated from the reaction mixture followed by the addition of H₂O (4 mL). The mixture was stirred for additional 2 min and then extracted with EtOAc (2 × 5 mL). The combined color extracts were

dried over anhydrous Na₂SO₄. Evaporation of the solvent under reduced pressure affords the pure crystals of azobenzene in 95% yield (0.077 g, Table 3, entry 1).

Conflicts of interest

The authors declare no conflicts of interest.

Acknowledgements

We gratefully acknowledge the financial support of this work by research councils of Urmia University.

References

- 1 K. Hunger, *Industrial Dyes: Chemistry, Properties, Applications*, Wiley-VCH, Weinheim, 2003.
- 2 H. Zollinger, *Colour Chemistry: Syntheses, Properties and Applications of Organic Dyes and Pigments*, Wiley-VCH, Switzerland, 3rd edn, 2003.
- 3 P. F. Gordon and P. Gregory, *Organic Chemistry in Colour*, Springer, New York, 1983, pp. 95–162.
- 4 R. D. Athey Jr, *Eur. Coat. J.*, 1998, **3**, 146.
- 5 P. N. D. Ashutosh and J. K. Mehrotra, *Colourage*, 1979, **26**, 25.
- 6 A. Jain, Y. Gupta and S. K. Jain, *Crit. Rev. Ther. Drug Carrier Syst.*, 2006, **23**, 349–400.
- 7 Z. F. Liu, K. Hashimoto and A. Fujishima, *Nature*, 1990, **347**, 658–660.
- 8 T. Ikeda and O. Tsutsumi, *Science*, 1995, **268**, 1873–1875.
- 9 H. Murakami, A. Kawabuchi, K. Kotoo, M. Kutinake and N. Nakashima, *J. Am. Chem. Soc.*, 1997, **119**, 7605–7606.
- 10 I. A. Banerjee, L. Yu and H. Matsui, *J. Am. Chem. Soc.*, 2003, **125**, 9542–9543.
- 11 F. Cisnetti, R. Ballardini, A. Credi, M. T. Gandolfi, S. Masiero, F. Negri, S. Pieraccini and G. P. Spada, *Chem.-Eur. J.*, 2004, **10**, 2011–2021.
- 12 J. C. Crano and R. J. Guglielmetti, *Organic Photochromic and Thermochromic Compounds*, Plenum Press, New York, 1999.
- 13 B. L. Feringa, R. A. van Delden, N. Koumura and E. M. Geertsema, *Chem. Rev.*, 2000, **100**, 1789–1816.
- 14 X. Liang, H. Asanuma and M. Komiyama, *J. Am. Chem. Soc.*, 2002, **124**, 1877–1883.
- 15 H. E. Zimmerman, R. J. Boettcher, N. E. Buehler, G. E. Keck and M. G. Steinmetz, *J. Am. Chem. Soc.*, 1976, **98**, 7680–7689.
- 16 B. M. Trost, R. M. Cory, P. H. Scudder and H. B. Neubold, *J. Am. Chem. Soc.*, 1973, **95**, 7813–7820.
- 17 K. Haghighi and E. W. Tan, *J. Org. Chem.*, 1998, **63**, 4503–4505.
- 18 H. D. Ansporn, *Org. Synth. Coll.*, 1955, **3**, 711.
- 19 E. Merino, *Chem. Soc. Rev.*, 2011, **40**, 3835–3853.
- 20 M. Rahimizadeh, H. Eshghi, A. Shiri, Z. Ghadamyari, M. M. Matin, F. Oroojalian and P. Pordeli, *J. Korean Chem. Soc.*, 2012, **56**, 716–719.
- 21 A. Zarei, A. R. Hajipour, L. Khazdooz, B. F. Mirjalili and A. N. Chermahini, *Dyes Pigment.*, 2009, **81**, 240–244.
- 22 A. Mitsutani, *Catal. Today*, 2002, **73**, 57–63.



- 23 J. Safari, S. H. Banitaba and S. D. Khalili, *J. Mol. Catal. A: Chem.*, 2011, **335**, 46–50.
- 24 A. Grirrane, A. Corma and H. Garcia, *Science*, 2008, **322**, 1661–1664.
- 25 C. Zhang and N. Jiao, *Angew. Chem., Int. Ed.*, 2010, **49**, 6174–6177.
- 26 X. Geng and C. Wang, *Org. Biomol. Chem.*, 2015, **13**, 7619–7623.
- 27 F. Ahmed Khan and C. Sudheer, *Tetrahedron Lett.*, 2009, **50**, 3394–3396.
- 28 Y. Lu, J. Liu, G. Diffie, D. Liu and B. Liu, *Tetrahedron Lett.*, 2006, **47**, 4597–4599.
- 29 J. R. Hwu, A. R. Das, C. W. Yang, J. J. Huang and M. H. Hsu, *Org. Lett.*, 2005, **7**, 3211–3214.
- 30 H. J. Shine and H. E. Mallory, *J. Org. Chem.*, 1962, **27**, 2390–2391.
- 31 H. W. Galbraith, E. F. Degering and E. F. Hitch, *J. Am. Chem. Soc.*, 1951, **73**, 1323–1324.
- 32 P. D. Ren, S. F. Pan, T. W. Dong and S. H. Wu, *Synth. Commun.*, 1996, **26**, 3903–3908.
- 33 T. F. Chung, Y. M. Wu and C. H. Cheng, *J. Org. Chem.*, 1984, **49**, 1215–1217.
- 34 S. Gowda and D. C. Gowda, *Synthesis*, 2002, 460–462.
- 35 G. R. Srinivasa, K. Abiraj and D. C. Gowda, *Synth. Commun.*, 2003, **33**, 4221–4227.
- 36 G. R. Srinivasa, K. Abiraj and D. C. Gowda, *Tetrahedron Lett.*, 2003, **44**, 5835–5837.
- 37 G. R. Srinivasa, K. Abiraj and D. C. Gowda, *Aust. J. Chem.*, 2004, **57**, 609–610.
- 38 R. F. Nystrom and W. G. Brown, *J. Am. Chem. Soc.*, 1948, **70**, 3738–3740.
- 39 J. F. Corbett, *Chem. Commun.*, 1968, 1257b–1258.
- 40 R. O. Hutchins, D. W. Lamson, L. Rua, C. Milewski and B. Maryanoff, *J. Org. Chem.*, 1971, **36**, 803–806.
- 41 A. C. Knipe, S. J. McGuinness and W. E. Watts, *J. Organomet. Chem.*, 1979, **172**, 463–466.
- 42 H. Alper and H. N. Paik, *J. Organomet. Chem.*, 1978, **144**, C18–C20.
- 43 W. Tadros, M. S. Ishak and E. Bassili, *J. Chem. Soc.*, 1959, 627–629.
- 44 A. Khan and S. Hecht, *Chem.–Eur. J.*, 2006, **12**, 4764–4774.
- 45 D. D. Laskar, D. Prajapati and J. S. Shandu, *J. Chem. Soc., Perkin Trans. 1*, 2000, **1**, 67–69.
- 46 M. B. Sridhara, R. Suhas and D. G. C. Gowda, *Eur. J. Chem.*, 2013, **1**, 61–63.
- 47 J. M. Khurana and A. Ray, *Bull. Chem. Soc. Jpn.*, 1996, **69**, 407–410.
- 48 P. Sobota, T. Pluzinski and S. Rummel, *Tetrahedron*, 1981, **37**, 939–942.
- 49 J. Wang, L. Hu, X. Cao, J. Lu, X. Li and H. Gu, *RSC Adv.*, 2013, **3**, 4899–4902.
- 50 N. Sakai, K. Fujii, S. Nabeshima, R. Ikeda and T. Konakahara, *Chem. Commun.*, 2010, **46**, 3173–3175.
- 51 N. Sakai, S. Asama, S. Anai and T. Konakahara, *Tetrahedron*, 2014, **70**, 2027–2033.
- 52 Y. Moglie, C. Vitale and G. Radivoy, *Tetrahedron Lett.*, 2008, **49**, 1828–1831.
- 53 C. Luo, X. Ji, S. Hou, N. Eidson, X. Fan, Y. Liang, T. Deng, J. Jiang and C. Wang, *Adv. Mater.*, 2018, **30**, e1706498.
- 54 H. Q. Li, X. Liu, Q. Zhang, S. S. Li, Y. M. Liu, H. Y. He and Y. Cao, *Chem. Commun.*, 2015, **51**, 11217–11220.
- 55 V. Kalyanaraman and M. V. George, *J. Org. Chem.*, 1973, **38**, 507–514.
- 56 S. Wada, M. Urano and H. Suzuki, *J. Org. Chem.*, 2002, **67**, 8254–8257.
- 57 J. A. Gladysz, J. G. Fulcher and S. Togashi, *Tetrahedron Lett.*, 1977, **18**, 521–524.
- 58 M. Tamura and H. Fujihara, *J. Am. Chem. Soc.*, 2003, **125**, 15742–15743.
- 59 V. K. Sharma, R. A. Yngard and Y. Lin, *Adv. Colloid Interface Sci.*, 2009, **145**, 83–96.
- 60 M. Nasrollahzadeh, S. M. Sajadi and A. Hatamifard, *J. Colloid Interface Sci.*, 2015, **460**, 146–153.
- 61 A. Hatamifard, M. Nasrollahzadeh and J. Lipkowski, *RSC Adv.*, 2015, **5**, 91372–91381.
- 62 M. Atarod, M. Nasrollahzadeh and S. M. Sajadi, *RSC Adv.*, 2015, **5**, 91532–91543.
- 63 M. Atarod, M. Nasrollahzadeh and S. M. Sajadi, *J. Colloid Interface Sci.*, 2016, **465**, 249–258.
- 64 M. Nasrollahzadeh, M. Maham, A. Rostami-Vartooni, M. Bagherzadeh and S. M. Sajadi, *RSC Adv.*, 2015, **5**, 64769–64780.
- 65 M. Nasrollahzadeh, S. M. Sajadi, A. Rostami-Vartooni, M. Alizadeh and M. Bagherzadeh, *J. Colloid Interface Sci.*, 2016, **466**, 360–368.
- 66 M. Nasrollahzadeh, *Tetrahedron Lett.*, 2016, **57**, 337–339.
- 67 M. Nasrollahzadeh, *New J. Chem.*, 2014, **38**, 5544–5550.
- 68 C. W. Lim and I. S. Lee, *Nano Today*, 2010, **5**, 412–434.
- 69 M. Nasrollahzadeh and S. M. Sajadi, *J. Colloid Interface Sci.*, 2016, **464**, 147–152.
- 70 Z. Shokri, B. Zeynizadeh and S. A. Hosseini, *J. Colloid Interface Sci.*, 2017, **485**, 99–105.
- 71 B. Zeynizadeh, I. Mohammadzadeh, Z. Shokri and S. A. Hosseini, *J. Colloid Interface Sci.*, 2017, **500**, 285–293.
- 72 Z. Shokri, B. Zeynizadeh, S. A. Hosseini and B. Azizi, *J. Iran. Chem. Soc.*, 2017, **14**, 101–109.
- 73 B. Zeynizadeh and F. Sepehraddin, *J. Iran. Chem. Soc.*, 2017, **14**, 2649–2657.
- 74 S. Karami, B. Zeynizadeh and Z. Shokri, *Cellulose*, 2018, **25**, 3295–3305.
- 75 B. Zeynizadeh and F. Sepehraddin, *J. Organomet. Chem.*, 2018, **856**, 70–77.
- 76 M. Gilanizadeh and B. Zeynizadeh, *New J. Chem.*, 2018, **42**, 8553–8566.
- 77 G. Y. Li, Y. R. Jiang, K. L. Huang, P. Ding and L. L. Yao, *Colloids Surf., A*, 2008, **320**, 11–18.
- 78 J. A. Lopez, F. Gonzalez, F. A. Bonilla, G. Zambrano and M. E. Gomez, *Rev. LatinAm. Metal. Mat.*, 2010, **30**, 60–66.
- 79 G. Zhang, T. Liu, T. Zhu, J. Qin, Y. Wu and C. Chen, *Opt. Mater.*, 2008, **31**, 110–113.

